



LAWRENCE
LIVERMORE
NATIONAL
LABORATORY

Deformation Twinning in a Creep-Deformed Nanolaminate Structure

L. L. Hsiung

July 13, 2010

Journal of Physics: Condensed Matter

Disclaimer

This document was prepared as an account of work sponsored by an agency of the United States government. Neither the United States government nor Lawrence Livermore National Security, LLC, nor any of their employees makes any warranty, expressed or implied, or assumes any legal liability or responsibility for the accuracy, completeness, or usefulness of any information, apparatus, product, or process disclosed, or represents that its use would not infringe privately owned rights. Reference herein to any specific commercial product, process, or service by trade name, trademark, manufacturer, or otherwise does not necessarily constitute or imply its endorsement, recommendation, or favoring by the United States government or Lawrence Livermore National Security, LLC. The views and opinions of authors expressed herein do not necessarily state or reflect those of the United States government or Lawrence Livermore National Security, LLC, and shall not be used for advertising or product endorsement purposes.

DEFORMATION TWINNING IN A CREEP-DEFORMED NANOLAMINATE STRUCTURE

Luke L. Hsiung*

Lawrence Livermore National Laboratory
Physical and Life Sciences Directorate
L-352, P.O. Box 808
Livermore, CA 94551-9900

Abstract - The underlying mechanism of deformation twinning occurred in a TiAl-(γ)/Ti₃Al-(α_2) nanolaminate creep-deformed at elevated temperatures has been studied. Since the multiplication and propagation of lattice dislocations in both γ and α_2 thin lamellae are very limited, the total flow of lattice dislocations becomes insufficient to accommodate the accumulated creep strains. Consequently, the movement of interfacial dislocations along the laminate interfaces, i.e., interface sliding, becomes an alternative deformation mode of the nanolaminate structure. Pile-ups of interfacial dislocations occur when interfacial ledges and impinged lattice dislocations act as obstacles to impede the movement of interfacial dislocations. Deformation twinning can accordingly take place to relieve a stress concentration resulting from the pile-up of interfacial dislocations. An interface-controlled twinning mechanism driven by the pile-up and dissociation of interfacial dislocations is accordingly proposed.

Keywords: Nanolaminate; interfacial dislocations; deformation twinning

Microstructure of TiAl-(γ)/Ti₃Al-(α_2) nanolaminate

Two-phase TiAl-(γ)/Ti₃Al-(α_2) nanolaminate material with nominal compositions (in at. %): Ti-47Al-2Cr-2Nb was used for this study. Detailed information regarding the powder metallurgy processing and the creep experiments for the TiAl-(γ)/Ti₃Al-(α_2) nanolaminate material has been reported elsewhere [1]. Figure 1a is a bright-field TEM image showing a typical edge-on microstructure of the nanolaminate. Note that TiAl-(γ) lamella is about 80 to 300 nm thick and has an ordered face-centered tetragonal structure (L1₀); Ti₃Al-(α_2) lamella is about 10 to 50 nm thick and has an ordered hexagonal close-packed structure (DO19).

* Corresponding author. Tel.: +1-925 424 3125; fax: +1-925 424 3815
E-mail address: hsiung1@llnl.gov

In general, the material contains two types of laminate interfaces [2]: (1) The γ/α_2 interphase interface that has an orientation relationship: $(0001)_{\alpha_2} \parallel (111)_{\gamma}$ and $\langle 11\bar{2}0 \rangle_{\alpha_2} \parallel \langle 1\bar{1}0 \rangle_{\gamma}$. (2) The γ/γ twin-related interface that includes true-twin (180° rotation) in which the $[\bar{1}10]$ direction of the matrix is anti-parallel to the $[\bar{1}10]$ direction of the twin, 120° rotational faults in which the $[\bar{1}10]$ direction of the matrix is parallel to the $[10\bar{1}]$ direction of the twin, and 60° pseudo-twins in which the $[\bar{1}10]$ direction of the matrix is anti-parallel to the $[10\bar{1}]$ direction of the twin. Figure 1b is a weak-beam dark-field (WBDF) TEM image showing a typical dislocation structure in the nanolaminate. Both lattice dislocations (LDs) in γ lamellae and interfacial dislocations (IDs) on inclined laminate interfaces can be clearly seen. The density of IDs is much greater than that of LDs, and the LDs are primarily threading dislocations which terminate their two ends at the interfaces. While the IDs in semi-coherent γ/α_2 and γ/γ pseudo-twin interfaces are $1/6\langle 112 \rangle$ -type misfit dislocations [3], the IDs in γ/γ true-twin interface are mainly $1/6[11\bar{2}]$ -type twin boundary dislocations for accommodating the departure of true-twin interface from the exact (111) twin plane. Figures 2a and 2b are high-resolution TEM (HRTEM) images showing the core structure of ID in γ/α_2 and γ/γ interfaces, respectively. Here each ID containing a small step (ledge) can be readily seen. The step height is $2d_{111}$ ($d_{111}=0.232$ nm) for the ID in γ/α_2 interface and is d_{111} for the ID in γ/γ interface

Dynamics of interfacial dislocations

Results of an in-situ TEM experiment directly observed the cooperative motion of IDs along laminate interfaces in a TiAl/Ti₃Al laminate under room-temperature straining conditions have been reported elsewhere [4]. The movement of IDs along laminate interface can be frequently blocked by impinged LDs, and a typical example is shown in Fig. 3. Here an array of IDs blocked by several impinged LDs in a γ/γ interface can be clearly seen. Figure 4 shows the result of another in-situ TEM experiment, in which the motion and pile-up of IDs were observed during an electron-beam heating of a thin foil that contains a residual stress. Note that the thin foil was prepared from a TiAl/Ti₃Al laminate creep-deformed to a total creep-stain of $\sim 0.25\%$ with a stress of 138 MPa at 760° C. It is also noted that the local heating was achieved by focusing the electron-beam to a spot size of several micron meters. Figure 4a shows the cooperative motion of a dislocation array of eight IDs in a laminate interface. The motion of each dislocation was in a viscous drifting or pinning/unpinning fashion, and each of them has a different drifting velocity. Here, after beam heating for 30 seconds, the #1 leading dislocation of the array moved about 375

nm, and the #8 trailing dislocation moved about 425 nm. This indicates that each ID moves with a different mobility as a result of a solute-dragging effect presumably caused by the segregation of solute (interstitial) atoms at laminate interfaces [5]. Figure 4b shows the motion of IDs in a dislocation pile-up along a laminate interface. Here, the head of dislocation pile-up is near to the tip of a faulted α_2 -lamella adjacent to the #1 dislocation. Notice that the dislocation spacing increases with increasing distance from the head of pile-up. In addition, the IDs near to the head of pile-up move slower than those IDs far away from the head of pile-up. For instance, after beam focusing (heating) for 30 seconds, #10 and #20 dislocations move about 170 nm; #35 and #45 dislocations move about 250 nm. Consequently, the beam heating causes the dislocation density in the pile-up further increases.

The above in-situ observations of ID motion and pile-up can be rationalized below. Since the thin foil still contains a residual shear stress (τ) that are acting on laminate interfaces, each ID starts to move under a heating condition with a velocity: $v = MF$, where M is the mobility of dislocation, and F is the effective force acting on each ID. An explicit expression for the dislocation mobility M limited by solute drag can be found in [6] is $M = \frac{D_s \Omega}{\beta b^2 C_0 k T}$, where β is a constant, b is the length of Burgers vector, C_0 is the solute

concentration and D_s is the solute diffusion coefficient, and Ω is the atomic volume of solute. For the effective force (F) acting on the i -th dislocation in a dislocation array or pile-up can be expressed as $F = \tau b - \frac{\mu b^2}{2\pi(1-\nu)} \sum_{\substack{j=0 \\ j \neq i}}^n \frac{1}{x_i - x_j}$ [7], where the term $\frac{\mu b^2}{2\pi(1-\nu)} \sum_{\substack{j=0 \\ j \neq i}}^n \frac{1}{x_i - x_j}$ represents the sum of repulsive forces acting on the i -th dislocation by the other dislocations in the pile-up; $x_i - x_j$ represents the distance between the i -th and j -th dislocations, and the 0th dislocation is the one adjacent to an insurmountable obstacle. Accordingly, v increases as a result of the increase in dislocation mobility as temperature (T) increases during beam heating, and v diminishes as temperature decreases to an ambient temperature. The velocity of dislocations near to the head of pile-up becomes slower indicates that the internal stress acting on the dislocations increases as the dislocations move closer to the head, which reduces the effective force (F) acting on the dislocations.

Interface-controlled deformation twinning

When a TiAl/Ti₃Al laminate was creep-deformed to a total creep-strain of ~3.6% with a constant stress of 518 MPa under a strain rate of $3 \times 10^{-7} \text{ s}^{-1}$ at 760 °C, a deformation structure associated with deformation

twins was developed in γ lamellae. Figure 5 shows typical $(\bar{1}11)$ [211]-type twins formed in γ lamellae. Here a twin lamella (marked by an arrow in Fig. 5a) nucleating from a laminate interface can be readily seen. It reveals that the laminate interfaces are the preferred sites for the nucleation of deformation twins in TiAl/Ti₃Al nanolaminate structure. The deformation twinning can relieve the local stress concentration resulting from the pile-up of IDs described above. The effective stress (τ_e) at the head of the pile-up of n dislocations can be evaluated as: $\tau_e = n\tau_i$ [8], where τ_i is the resolved shear stress acting on the interface. To relieve the stress concentration, deformation twinning in γ layers takes place by a dislocation reaction based upon a stair-rod cross-slip mechanism as schematically illustrated in Fig. 5b. For the formation of a $(\bar{1}11)$ -type twin lamella, the corresponding dislocation reaction is $1/6[\bar{1}2\bar{1}]_{(111)} [\mathbf{b1}] \rightarrow 1/6[011]_{(100)} [\mathbf{b2}] + 1/6[\bar{1}1\bar{2}]_{(\bar{1}11)} [\mathbf{b3}]$. The $(\bar{1}11)$ -type twin is accordingly formed in γ lamella by successively dissociating the $[\mathbf{b1}]$ IDs in the pile-up and emitting the $[\mathbf{b3}]$ twinning dislocations into the $(\bar{1}11)$ plane and leaving the $[\mathbf{b2}]$ stair-rod dislocations in the (100) plane. Figures 5c and 5d show several edge-on twin lamellae; the widths of twin lamellae were measured to be ranging from 3 nm and 20 nm. The formation of $[\mathbf{b2}]$ stair-rod dislocations and $[\mathbf{b3}]$ twinning dislocations was verified using the \mathbf{g} (reflection vector) $\cdot \mathbf{b}$ (Burger's vector) contrast-visibility analyses [9], and the results are shown in Fig. 6. Here the arrays of $1/6[011] [\mathbf{b2}]$ stair-rod dislocations formed at the junctions between twin and α_2 lamellae are invisible (Fig. 6a) or visible (Fig. 6b) when $\mathbf{g} = 200$ or $\mathbf{g} = 021$ is used for imaging; the arrays of $1/6[112](11\bar{1}) [\mathbf{b3}]$ twinning dislocations formed at the junctions between twin and γ lamellae are visible (Fig. 6c) or invisible (Fig. 6d) when $\mathbf{g} = 111$ or $\mathbf{g} = 20\bar{2}$ is used for imaging. It is noted that an individual stair-rod dislocation cannot be resolved due to a very small distance (0.25 nm) between two stair-rod dislocations, which is much smaller than the resolution limit (1 nm) obtained under weak-beam imaging conditions.

The above observations suggest that two critical barriers have to be overcome to onset the interface-controlled deformation twinning, which include 1) the repulsive force between interfacial (Shockley) and stair-rod dislocations and 2) the increase of interfacial energy due to the formation of twin lamella. Among which the repulsive force (F) between the interfacial (Shockley) and stair-rod dislocations is considered to be the rate-limiting process. That is, a threshold stress (τ_c) is required to onset the twinning reaction. Assuming an isotropic elasticity, the threshold stress (τ_c) can be approximately evaluated as: $\tau_c b_1 = \eta \mu b_1 b_2 \cos\theta / 2\pi r$, where, $\eta = 1$ for screw dislocations and $\eta = 1/(1-\nu)$ for edge dislocations, and ν is Poisson's ratio (~ 0.3); μ is

shear modulus (~ 56 GPa at 760°C [10]), $b_1 = 0.163$ nm, and $b_2 = 0.094$ nm for Shockley and stair-rod dislocations, respectively; θ ($= 54.4^\circ$) is the angle between $(\bar{1}11)$ and (100) planes, and r (0.25 nm) is the distance between the two dislocations. Accordingly, the threshold stress (τ_c) required for twinning is 1.95 GPa for the screw-type IDs and is 2.79 GPa for the edge-type IDs. The threshold stress is clearly much higher than the resolved shear stress (< 259 MPa) acting on the laminate interfaces. An internal stress resulting from the pile-up of dislocations is accordingly required to onset the interface-controlled deformation twinning.

Conclusions

Deformation twinning, which occurs in a creep-deformed TiAl/Ti₃Al nanolaminate, is found to be intimately related to the glide, pile-up, and dissociation of interfacial dislocations in laminate interfaces. When the arrays of interfacial (e.g. $1/6\langle 112 \rangle$ Shockley partial) dislocations move along the interfaces, they encounter obstacles such as impinged lattice dislocations and interfacial ledges. The dislocation arrays start to pile-up behind an insurmountable obstacle since an individual Shockley partial is energetically unfavorable to undergo cross-slip or climb that otherwise will generate stacking fault on its wake if it moves away from the interface. Thus, the arrays of interfacial (Shockley partial) dislocations can easily pile-up even at elevated temperatures. The deformation twinning in the creep-deformed nanolaminate can be rationalized as a relaxation process to dissipate the stress concentration resulting from the pile-up of interfacial dislocations. The twinning reaction involves the dissociation of interfacial dislocations into stair-rod (or residual) and twinning dislocations, i.e. $1/6[\bar{1}2\bar{1}]_{(111)} \rightarrow 1/6[011]_{(100)} + 1/6[\bar{1}1\bar{2}]_{(\bar{1}11)}$ for the $(\bar{1}11)[\bar{1}1\bar{2}]$ -type twinning. The development of dislocation pile-up configuration is a prerequisite condition to onset deformation twinning, which is most likely to occur under low-temperature and high strain-rate conditions for monolithic metals and alloys. The occurrence of deformation twinning in a creep-deformed TiAl/Ti₃Al nanolaminate indicates that the pile-up configuration of interfacial ($1/6\langle 112 \rangle$ Shockley partial) dislocations can be sustained even at elevated temperatures.

Acknowledgments

This work was performed under the auspices of the U.S. Department of Energy by Lawrence Livermore National Laboratory under Contract DE-AC52-07NA27344. The author gratefully acknowledges Dr. C.T. Liu for supplying TiAl/Ti₃Al laminate material.

References

1. L. M. Hsiung, T. G. Nieh, *Mater. Sci. & Engrg.* **A364**, p. 1 (2004).
2. M. Yamaguchi and Y. Umakoshi, *Progress in Materials Science*, **34**, p. 1 (1990).
3. G. J. Mahon, J. H. Howe, *Metall. Trans. A*, **21A**, p. 1655 (1990).
4. L. M. Hsiung, J. Zhou, and T. G. Nieh, *J. of Mater. Res.* **21**, p. 2453 (2006).
5. L. M. Hsiung, T. G. Nieh, *Intermetallics* **7**, p. 821 (1999).
6. E. Arzt, M.F. Ashby, R.A. Verrall, *Acta Metall.* **31**, p. 1977 (1983).
7. J. Weertman, *J. Appl. Phys.* **28**, p. 1185 (1957).
8. J. D. Eshelby, F. C. Frank, F. R. N. Nabarro, *Phil. Mag.*, **42**, p. 351 (1951).
9. J. W. Edington, *Practical Electron Microscopy in Materials Science*, Van Nostrand Reinhold, New York, 1976.
10. S. C. Huang, J. C. Chesnutt, *Intermetallic Compounds: Principles and Practice 2*, ed. J. H. Westbrook and R. L. Fleischer, John Wiley & Sons, p. 73 (1995).

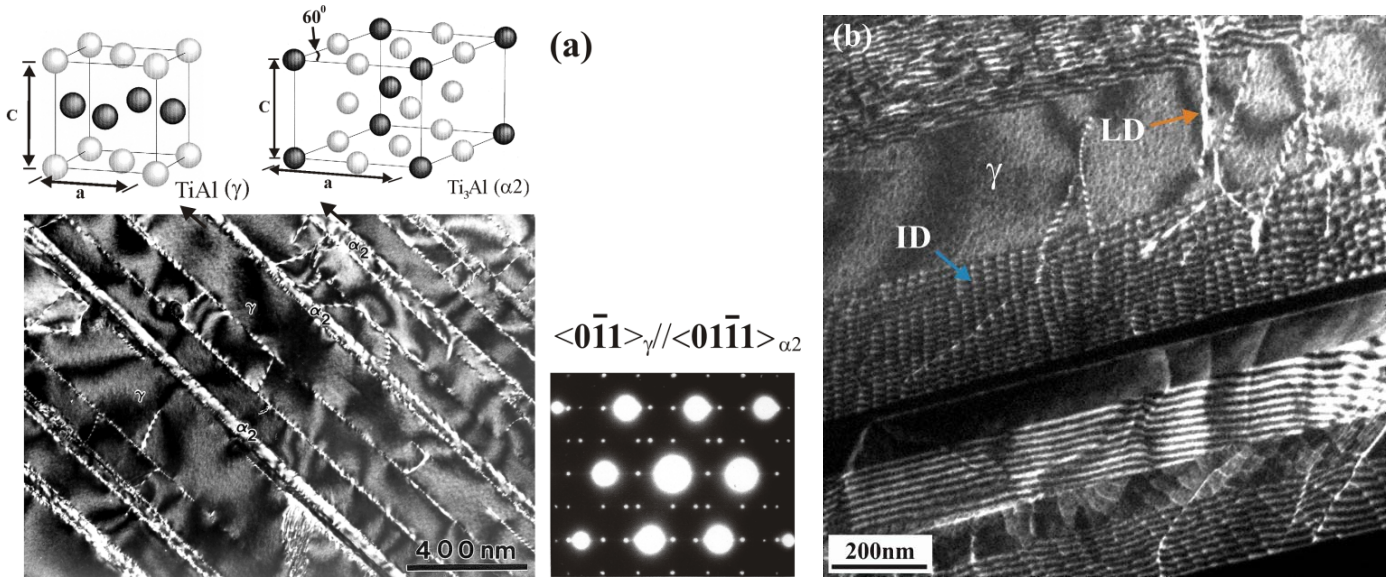


Fig. 1. (a) A bright-field TEM image shows a TiAl/Ti₃Al laminate viewing from an edge-on orientation, i.e. $\langle 0\bar{1}1 \rangle_{\gamma} \parallel \langle 01\bar{1}0 \rangle_{\alpha_2}$; (b) A WBDF TEM image shows a typical microstructure of lattice dislocations (LD) and interfacial dislocations (ID) in a TiAl/Ti₃Al nanolaminate.

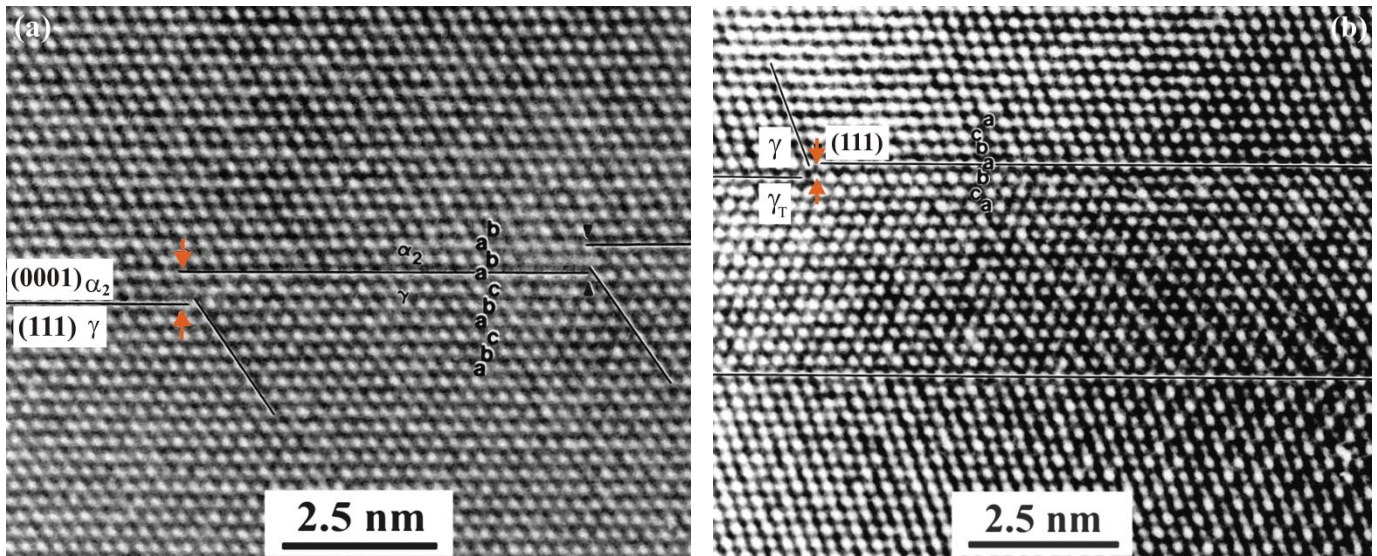


Fig. 2. High-resolution TEM (HRTEM) images show core structure of the $1/6\langle 112 \rangle$ ID in (a) γ/α_2 interphase interface and (b) γ/γ twin-related interface. The letters **abab** and **abcbabc** stand for the stacking sequence of atoms in α_2 and γ lamellae, respectively.

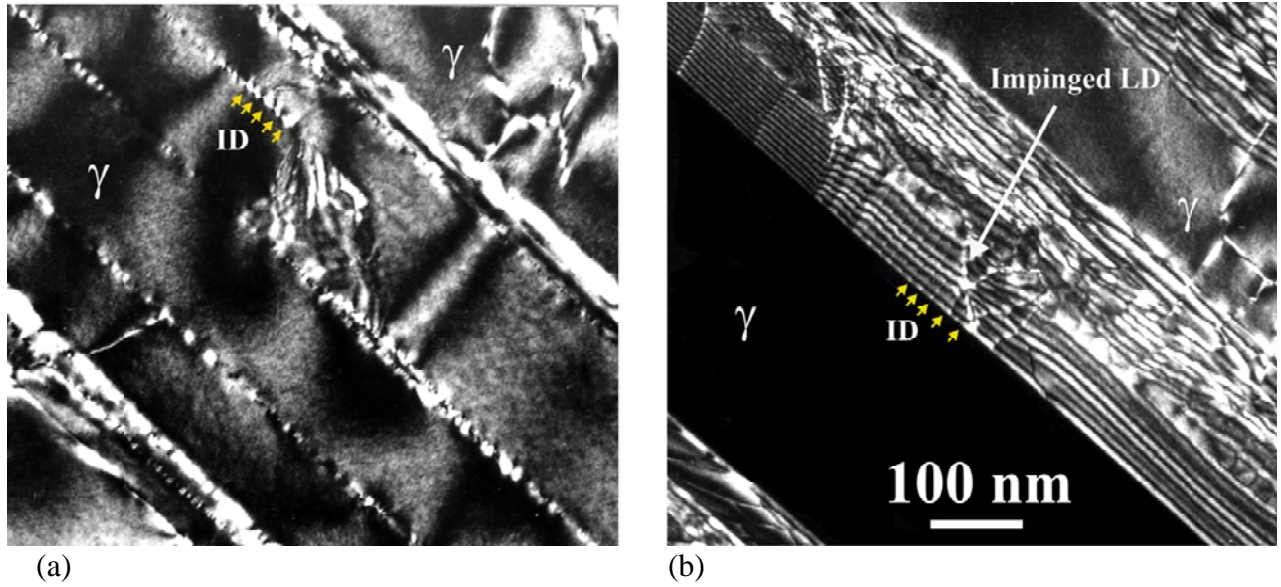


Fig. 3. WBDF TEM images show that the movement of IDs (marked by small arrows) is impeded by impinging LDs; (a) an edge-on view and (b) an inclined view of laminate interfaces.

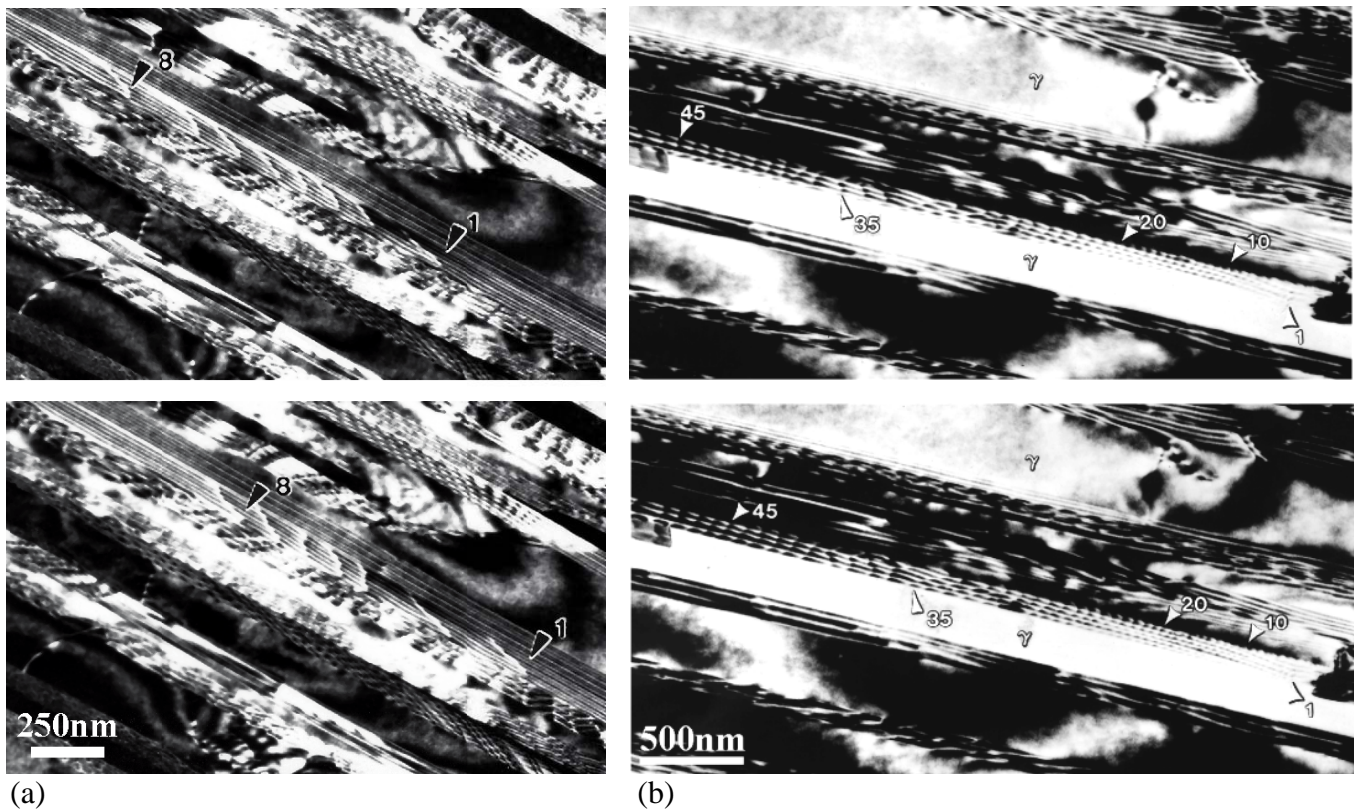


Fig. 4. Consecutive in-situ TEM images show that (a) the movement of an ID array in a laminate interface (time span: 30 seconds), and (b) the movement and pile-up of an ID array in a laminate interface adjacent to the tip of a faulted α_2 -lamella (time span: 30 seconds).

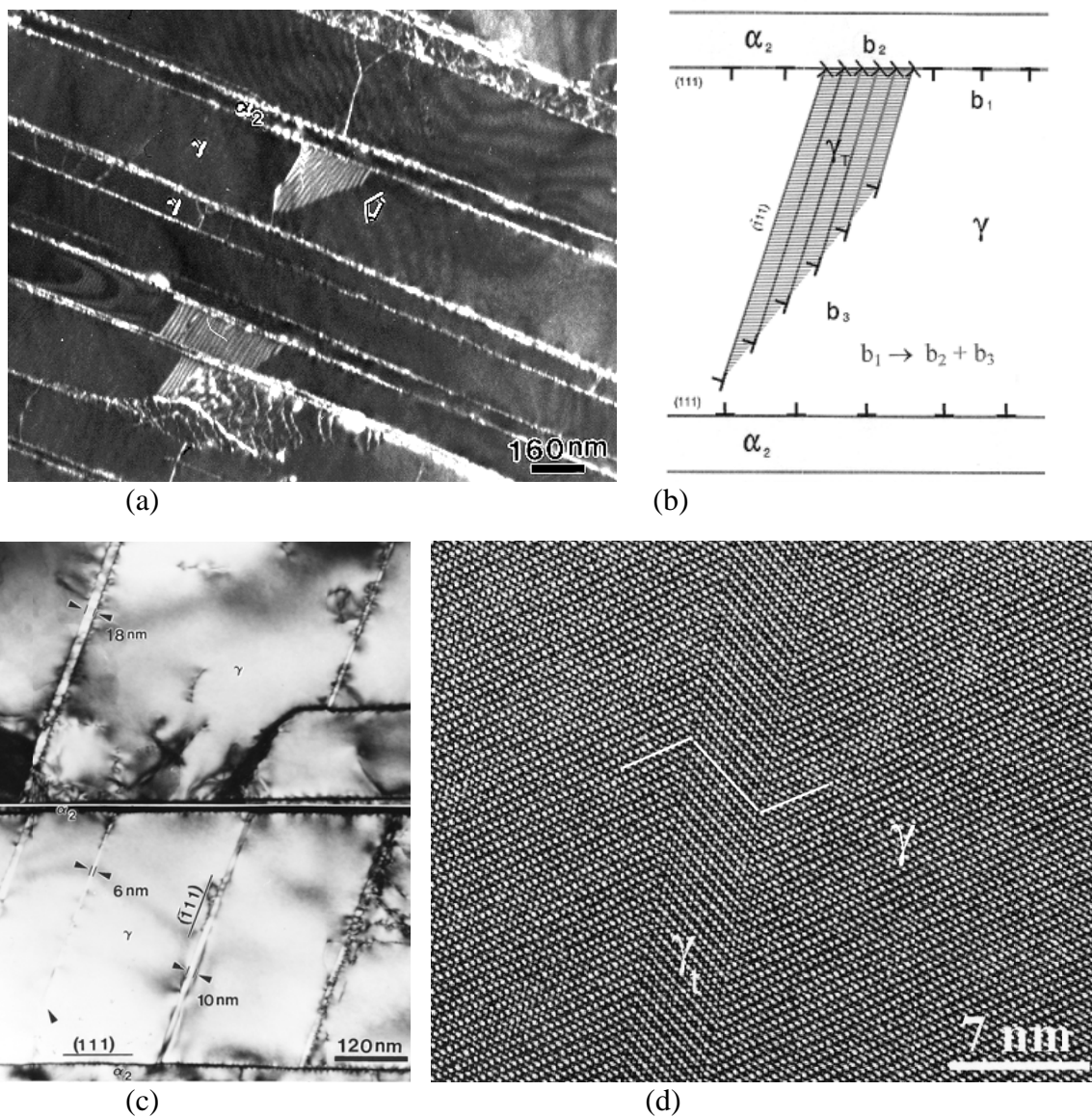


Fig. 5. (a) A dark-field TEM image shows the $(\bar{1}11)$ -type twin lamellae formed in γ lamellae; (b) A schematic illustration of the nucleation of a $(\bar{1}11)$ -type twin lamella (γ_t) from a γ/α_2 interface, where b_1 , b_2 , and b_3 denote the interfacial, stair-rod, and twinning dislocations, respectively; (c) Edge-on, \mathbf{Z} (zone axis) = $[0\bar{1}1]_\gamma$, views reveal the widths of nanometer-sized twin lamellae; (d) HRTEM image of an edge-on twin lamella.



Fig. 6. WBDF TEM images show the $\mathbf{g}\cdot\mathbf{b}$ contrast visibility analyses for the formation of $1/6[011](100)$ $[\mathbf{b}2]$ stair-rod dislocations and the $1/6[112](11\bar{1})$ $[\mathbf{b}3]$ twinning dislocations; (a) $[\mathbf{b}2]$ dislocations are invisible at $\mathbf{g} = 200$ ($\mathbf{g}\cdot\mathbf{b} = 0$), and (b) $[\mathbf{b}2]$ dislocations are visible at $\mathbf{g} = 021$ ($\mathbf{g}\cdot\mathbf{b} = 1/2$), $\mathbf{Z} \approx [0\bar{1}2]_{\gamma}$; (c) $[\mathbf{b}3]$ dislocations are visible at $\mathbf{g} = 111$ ($\mathbf{g}\cdot\mathbf{b} = 2/3$), and (d) $[\mathbf{b}3]$ dislocations are invisible at $\mathbf{g} = 20\bar{2}$ ($\mathbf{g}\cdot\mathbf{b} = 1/3$), \mathbf{Z} (zone axis) $\approx [1\bar{2}1]_{\gamma}$.